PHYSICAL REVIEW E **82**, 015305(R) (2010)

Capillary force repels coffee-ring effect

Byung Mook Weon[1,*] and Jung Ho Je[2,†]
[1]*Department of Physics, School of Engineering and Applied Sciences, Harvard University, Cambridge, Massachusetts 02138, USA*
[2]*X-ray Imaging Center, Department of Materials Science and Engineering, Pohang University of Science and Technology, Pohang 790-784, Korea*

(Received 24 March 2010; revised manuscript received 19 May 2010; published 26 July 2010)

When a coffee drop dries on a solid surface, it leaves a ringlike deposit along the edge and this is known as the "coffee-ring effect." We find a different motion of particles repelling the coffee-ring effect in drying droplets; the motion of particles that is initially toward the edge by the coffee-ring effect is reversed toward the center by a capillary force. The reversal takes place when the capillary force prevails over the outward coffee-ring flow. We discuss the geometric constraints for the capillary force and the reverse motion. Our findings of reversal phenomena would be important in many scenarios of drying colloidal fluids.

DOI: 10.1103/PhysRevE.82.015305 PACS number(s): 47.54.−r, 47.55.nb, 47.57.−s, 68.03.Fg

The coffee-ring effect—the tendency for solute to segregate at the edge—well explains how the net *outward* fluid flow on liquid-substrate interface forms a ringlike deposit near the periphery [1–4]. This effect is due to the nonuniform evaporation flux, which induces the fluid flow to replenish the evaporation loss at the edge [1,4]. However, the coffee-ring deposition does not explain the drying-mediated *inward* transport of particles in a variety of suspensions including colloidal fluids and DNA droplets. As one of the examples, the Marangoni effect (the surface-tension gradient) can reverse the coffee-ring effect [3–5]. A full understanding of the coffee-ring and the reverse effects is of vital importance to resolve many problems in pure science and in emerging technologies such as DNA stretching [6–8], pattern (multiple-ring) formation [9–12], and colloidal self-assembly [13–15].

We describe here a quite different tendency of solute to segregate at the center of drying droplets. The phenomenon is primarily driven by geometric constraints, instead of typical transport mechanisms such as surface-tension gradients, solute diffusion, electrostatic, and gravity effects. Precise tracking of particle motion and contact line in drying droplets was obtained with real-time optical, x-ray, and confocal microscopes. We argue that particle motion, initially toward the edge, can be reversed to the center by a capillary force [16,17]. The force is a kind of lateral immersion capillary force [16], which works when the particles get in contact with the air-liquid interface during evaporation. This effect is predictable and controllable from the geometric constraints of droplet and particles.

A typical result providing evidence for the unique effect is shown in Fig. 1. We observe a clear inward migration of 20-μm-diameter polystyrene (PS) microspheres (density $\rho_{PS}=1.05$ g cm^{-3}) suspended in a drying water droplet ($\rho_w=0.998$ g cm^{-3}) on a solid substrate (Petri dish). Sequential optical micrographs [18] were superimposed (with the IMAGE-PRO PLUS software) to reveal the inward motion during the droplet evaporation. Tracking the motion for about 140 s, we observed that most microspheres moved first toward the edge and then back toward the center. The standard effect [1,2] in the first phase produced ringlike stains near the periphery. We also found the reverse effect in various PS and silica microspheres in water or in coffee droplets. The subsequent inward migration of the microspheres in water is a unique transport phenomenon, different from the standard effect [1,2] or the Marangoni effect [3,5].

The phenomenon was found to depend on the particle size. A series of real-time optical micrographs clearly illustrate this size dependence for particles suspended in water [a droplet of ~1.5 mm diameter; Fig. 2(a)]. The results concern both 2- and 20-μm-diameter PS microspheres and are shown for different drying times t (with the complete evaporation time t_0 set to zero). The motion of the large particles is initially toward the edge but reversed to the center later on. The reversal is faster for the particles closer to the edge. On a contrary, most of the small particles tend to move constantly near the edge, forming ringlike stains. This picture suggests that the reversal motion of particles is much easier for large particles than for small ones.

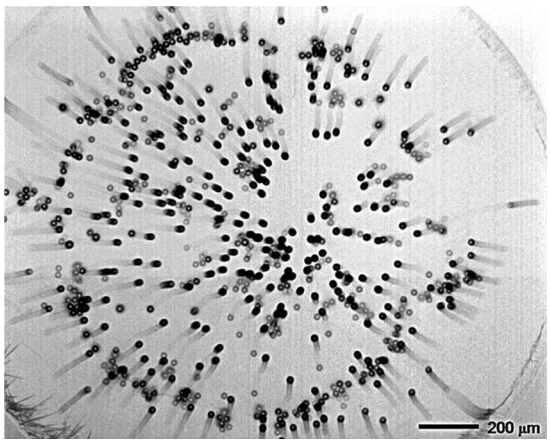

FIG. 1. Typical results providing evidence for the reverse motion of particles. Sequential optical micrographs [18] were superimposed to reveal the motion of microspheres. We observe an inward migration of 20-μm-diameter polystyrene microspheres suspended in a drying water droplet on a solid substrate (Petri dish). This reverse motion phase was preceded by the formation of ringlike stains at the perimeter by the normal coffee-ring effect.

*bmweon@hotmail.com
†jhje@postech.ac.kr

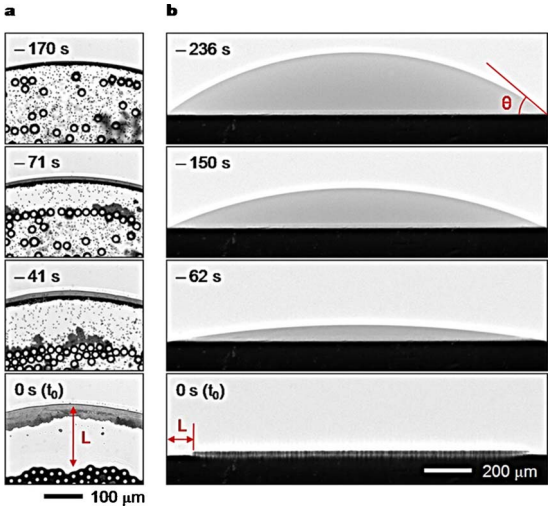

FIG. 2. (Color online) Real-time optical and x-ray micrographs. (a) Top-view optical micrographs show the normal and reverse motions of 2- and 20-μm-diameter particles in an evaporating water droplet of 1.5 mm diameter. (b) Side-view x-ray micrographs show the gradual reduction in the contact angle with the evaporation time for a water droplet suspension under the same conditions as (a). The reverse motion distance L from the edge increases with time, depending on the particle size and the contact angle.

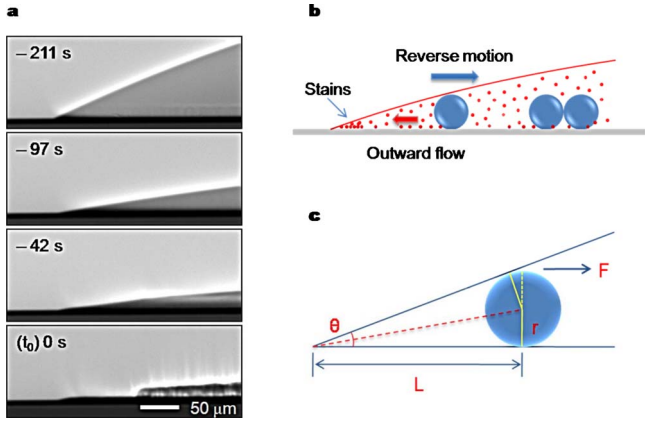

FIG. 3. (Color online) Capillary force leading to reverse motion. (a) High-resolution x-ray micrographs in the vicinity of the droplet edge. No protrusion of particles indicates the presence of capillary force during evaporation. (b) A schematic view of the capillary force explaining the reverse motion. (c) Geometric model of the reverse motion. A relation $\tan(\theta/2)=r/L$ links the particle radius r, the reverse moving distance L, and the contact angle θ. The increase in L is caused by the net capillary force F and is directly related to the contact angle evolution.

We present real-time x-ray micrographs showing the meniscus evolution of a drying water droplet [Fig. 2(b)]. Precise tracking of the air-water interface was made possible by phase contrast microradiography [19–21]. We employ hard x rays from a synchrotron source (7B2 beam line, Pohang Light Source, Korea [20]) (dose rate of ~ 1 kGy s^{-1}) to obtain clear images from a thick sample. High-flux, spatially coherent, and hard x rays (photon energy of $\sim 10-60$ keV) are effective in delineating interfaces in multiphase systems with a submicrometer-level accuracy [20]. This imaging clearly shows the geometric constraints of the droplet that determine the reverse particle motion: (i) the free liquid surface, (ii) the pinned contact line, and (iii) the contact angle that gradually decreases with evaporation; these are the same elements that characterize the normal coffee-ring effect [1,2]. Specifically, the average motion distance L of large particles from the periphery increases with drying time until the motion is limited to the close packing at the center. Obviously, the time evolution of L depends on the particle size [Fig. 2(a)] and on the contact angle evolution [Fig. 2(b)]. Indeed, we argue that the geometric evolution of the drying droplet is a crucial factor in the reversal motion of particles.

We first notice that there is no protrusion of particles from the droplet surface during evaporation even when the height of the droplet surface becomes lower than the particle size, as shown by the x-ray micrographs in Fig. 3(a). No protrusion suggests the existence of a capillary force working on the moving particles. The reverse motion of particles can be explained by the net capillary force between liquid surface and particles [16,17]. Particularly, the reversal happens whenever the inward force caused by the capillary force prevails over the outward flow by the coffee-ring effect. The capillary force as schematically illustrated in Fig. 3(b) can play a significant role in the reverse motion. The magnitude of the force, which is related to the wetting property of the particle surface, can be significant as one of the main factors causing self-assembly of small colloidal particles and protein macromolecules confined in thin liquid films [16]. Capillary force acting on micron-sized particles is much larger than thermal energy (~ 1 pN$\sim 10^3 k_B T/r$) [17] and capillary pressure from the curvature around the particles typically exceeds atmospheric pressure [22]. A geometric relation in Fig. 3(c) shows that the capillary force depends on the particle size and the contact angle. The reverse motion distance L from the edge, caused by the net capillary force F, increases as the particle size increases or as the contact angle decreases. We argue that the capillary force relates to a geometric relation $\tan(\theta/2)=r/L$, with the particle radius r and the contact angle θ, assuming no protrusion of particles as well as contact-line pinning. As seen in Fig. 2, the reverse motion distance L and the contact angle θ change with evaporation time, whereas the particle radius r is constant. The reverse motion dynamics is thus expected to relate with the contact angle evolution.

We now discuss the dynamics of the reverse motion. The reverse motion distance and the contact angle were, respectively, measured from real-time optical and x-ray micrographs. A power-law time dependence of $\theta(t)=\theta_0(t_0-t)^\beta$ is empirically observed for the contact angle evolution. The power law is typical for evaporating water droplets on a solid substrate when the contact line is pinned (see Ref. [23]). The tangent evolution of the contact angle can be simplified as $\tan[\theta(t)]\sim\theta(t)$ [radian] at small angles (typically $<30°$). The geometric relation based on the capillary force is then $L(t)=r/\tan[\theta(t)/2]\approx 2r/\theta(t)\approx(2r/\theta_0)(t_0-t)^{-\beta}$. The reverse motion distance is therefore expected to exhibit an inverse power-law scaling,

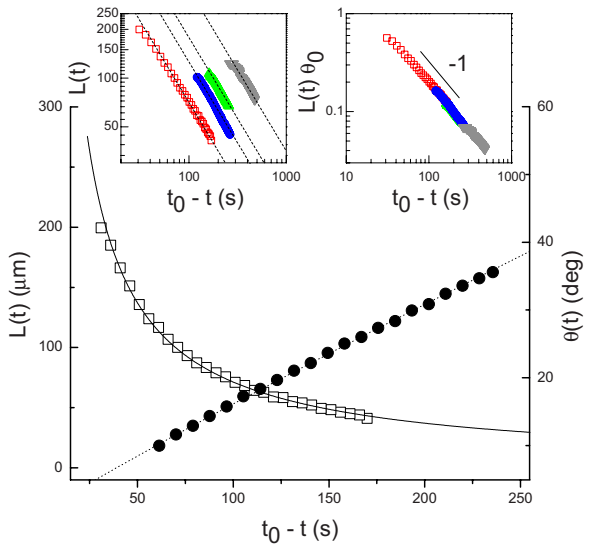

FIG. 4. (Color online) Correlation of the moving distance and the contact angle. The distance $L(t)$ (open squares) and the angle $\theta(t)$ (solid circles) were measured from the real-time optical [Fig. 2(a)] and x-ray [Fig. 2(b)] micrographs, respectively. The capillary force is predicted to lead to an inverse power-law increase in the moving distance $L(t)$ from the edge. The measured contact angle $\theta(t)$ that decreases with time $(t \rightarrow t_0)$ follows a power-law dependence as $\theta(t) \approx \theta_0(t_0-t)^{\beta}$ (dotted line). The measured moving distance in fact follows the inverse power law $L(t) \approx L_0(t_0-t)^{-\alpha} \approx (2r/\theta_0)(t_0-t)^{-\beta}$ (solid line). The inverse power law $L(t)$ applies even for different droplet sizes, as shown by the dashed lines in the left inset, reporting results for (from left to right) 1.5-, 2.0-, 2.5-, and 4.0-mm-diameter drops. The power law $L(t)\theta_0 \approx 2r(t_0-t)^{-1}$ is rescaled for different drop sizes with different θ_0 values in the right inset.

$$L(t) \approx L_0(t_0 - t)^{-\alpha}.$$

Here, $L(t)$ is a function of the prefactor L_0 and the exponent α for the evaporation time (t_0-t). Indeed, the evolution of $L(t)$ (squares in Fig. 4) follows an inverse power-law function (solid line). The exponent α $(=0.942 \pm 0.008)$ is approximately equal to the exponent β $(=0.935 \pm 0.005)$, and the prefactor L_0 (=5467) is approximately equal to the value of $2r/\theta_0$ (=5405) with $r=10$ μm and $\theta_0=0.0037$. Here, β and θ_0 were obtained by best fitting the time dependence of the contact angle (circles). The coincidence of $\alpha \approx \beta$ and $L_0 \approx 2r/\theta_0$ suggests that the inverse power-law growth of $L(t)$ is related to the power-law reduction in $\theta(t)$. The inverse power-law growth of $L(t)$ applies even for different drop sizes, D_{drop}, as indicated by the dashed lines with a power of -1 in the left inset of Fig. 4 (from the left to the right, $D_{\mathrm{drop}}=1.5$-, 2.0-, 2.5-, and 4.0-mm-diameter drops). Here, since the prefactor θ_0 in $L(t) \approx (2r/\theta_0)(t_0-t)^{-1}$ depends on the drop size, we rescale $L(t)\theta_0 \approx 2r(t_0-t)^{-1}$ in the right inset of Fig. 4, where the trajectories are coincident. This result implies that the inverse power law of $L(t)$ is mostly related to the particle size and the contact angle when the contact line gets pinned and the capillary force drives particles to move to the center.

The above analysis predicts that the motion can significantly change with the particle size in a given droplet. This leads to the separation of particles with different sizes as observed in Fig. 2(a): large particles tend to segregate near the center, while small particles tend to segregate at the edge. A similar particle separation was also reported in a recent experiment [24]. This may open a new way to control particle separation with many different potential applications.

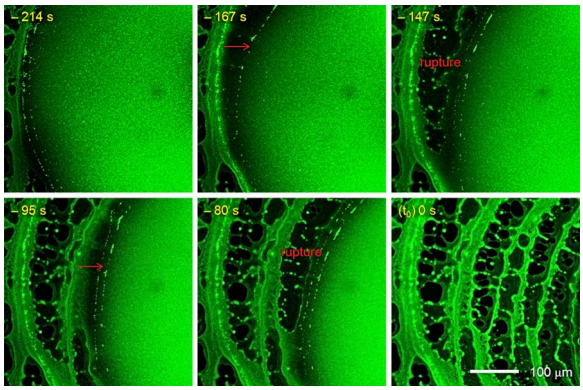

FIG. 5. (Color online) Confocal micrographs of multiple-ring formation. Multiple rings were formed from a mixture of 3.6- and 0.2-μm-diameter fluorescently labeled PMMA particles in decalin on a clean cover glass. Sequential confocal images [18] taken for an evaporating droplet of the suspension show that the reverse motion (marked by the arrow and revealed by the bright ring of large particles) sweeps the particles toward the center and stops by rupture. The repeated events result in the multiple-ring formation.

The reverse particle motion can strongly affect the pattern (multiple-ring) formation. In fact we observed multiple rings in a mixture of 3.6- and 0.2-μm-diameter fluorescently labeled PMMA (polymethylmethacrylate) particles using confocal microscopy. We used a mixture of PMMA particles (density $\rho_{\mathrm{PMMA}}=1.19$ g cm^{-3} and index of refraction $n_{\mathrm{PMMA}}=1.49$) suspended in decalin ($\rho_{\mathrm{dec}}=0.897$ g cm^{-3} and $n_{\mathrm{dec}}=1.48$) [22]. Here, samples were dried on clean glass substrates with an initial volume fraction of about 1%. A sequence of confocal images [18] was taken for an evaporating droplet (1 μl) of the suspension as demonstrated in Fig. 5. A bright ring initially formed at the edge with large particles partly moves toward the center by the capillary force as marked by the arrow. A new deposit ring is formed when the reverse motion is stopped by rupture. This event repeatedly occurs and multiple rings are thus generated by the competition between the normal coffee-ring and the reverse effects. The same mechanism may explain the multiple-ring formation in DNA and colloidal droplets [7,9,10].

In conclusion, we show a mechanism of reverse particle motion that repels the coffee-ring effect because of the capillary force near the contact line. From real-time monitoring of particle motion and contact line in drying droplets with optical, x-ray, and confocal microscopes, we suggest the geometric constraints for this phenomenon. The reverse motion by the capillary force may find interesting applications besides the separation of particles with different sizes. In combination with the normal coffee-ring effect, such reversal phenomena may play an important role in pure science and

in emerging technologies such as the deposition of DNA and RNA microarrays, spotting methods for gene mapping, drug discovery, and manufacturing of novel electronic and optical architectures, including thin films and coatings [16].

We thank D. A. Weitz and L. Xu for valuable comments on the early manuscript. This research was supported by the Creative Research Initiatives (Functional X-ray Imaging) of MEST/NRF.

[1] R. D. Deegan, O. Bakajin, T. F. Dupont, G. Huber, S. R. Nagel, and T. A. Witten, Nature (London) **389**, 827 (1997).
[2] R. D. Deegan, O. Bakajin, T. F. Dupont, G. Huber, S. R. Nagel, and T. A. Witten, Phys. Rev. E **62**, 756 (2000).
[3] H. Hu and R. G. Larson, J. Phys. Chem. B **110**, 7090 (2006).
[4] W. D. Ristenpart, P. G. Kim, C. Domingues, J. Wan, and H. A. Stone, Phys. Rev. Lett. **99**, 234502 (2007).
[5] X. Xu and J. Luo, Appl. Phys. Lett. **91**, 124102 (2007).
[6] S. S. Abramchuk, A. R. Khokhlov, and T. Iwataki, EPL **55**, 294 (2001).
[7] X. Fang, B. Li, E. Petersen, Y.-S. Seo, V. A. Samuilov, Y. Chen, J. C. Sokolov, C.-Y. Shew, and M. H. Rafailovich, Langmuir **22**, 6308 (2006).
[8] I. I. Smalyukh, O. V. Zribi, J. C. Butler, O. D. Lavrentovich, and G. C. L. Wong, Phys. Rev. Lett. **96**, 177801 (2006).
[9] R. D. Deegan, Phys. Rev. E **61**, 475 (2000).
[10] V. X. Nguyen and K. J. Stebe, Phys. Rev. Lett. **88**, 164501 (2002).
[11] L. Shmuylovich, A. Q. Shen, and H. A. Stone, Langmuir **18**, 3441 (2002).
[12] S. Maheshwari, L. Zhang, Y. Zhu, and H.-C. Chang, Phys. Rev. Lett. **100**, 044503 (2008).
[13] M. H. Kim, S. H. Im, and O. O. Park, Adv. Funct. Mater. **15**, 1329 (2005).
[14] Z. Lin and S. Granick, J. Am. Chem. Soc. **127**, 2816 (2005).
[15] J. Xu, J. Xia, S. W. Hong, Z. Lin, F. Qiu, and Y. Yang, Phys. Rev. Lett. **96**, 066104 (2006).
[16] P. A. Kralchevsky and N. D. Denkov, Curr. Opin. Colloid Interface Sci. **6**, 383 (2001).
[17] R. Di Leonardo, F. Saglimbeni, and G. Ruocco, Phys. Rev. Lett. **100**, 106103 (2008).
[18] See supplementary material at http://link.aps.org/supplemental/10.1103/PhysRevE.82.015305 for movies of the reverse particle motion or the multiple-ring formation.
[19] W. L. Tsai, P. C. Hsu, Y. Hwu, C. H. Chen, L. W. Chang, J. H. Je, H. M. Lin, A. Groso, and G. Margaritondo, Nature (London) **417**, 139 (2002).
[20] B. M. Weon, J. H. Je, Y. Hwu, and G. Margaritondo, Phys. Rev. Lett. **100**, 217403 (2008).
[21] B. M. Weon, J. H. Je, Y. Hwu, and G. Margaritondo, J. Synchrotron Radiat. **15**, 660 (2008).
[22] L. Xu, S. Davies, A. B. Schofield, and D. A. Weitz, Phys. Rev. Lett. **101**, 094502 (2008).
[23] C. Poulard, O. Benichou, and A. M. Cazabat, Langmuir **19**, 8828 (2003).
[24] A. S. Sangani, C. Lu, K. Su, and J. A. Schwarz, Phys. Rev. E **80**, 011603 (2009).